Available online at www.sciencedirect.com
SCIENCE DIRECT
Journal of Catalysis 227 (2004) 479–491
JOURNAL OF CATALYSIS
www.elsevier.com/locate/jcat

Support effects on Brønsted acid site densities and alcohol dehydration turnover rates on tungsten oxide domains

Josef Macht [a], Chelsey D. Baertsch [a], Marcos May-Lozano [a], Stuart L. Soled [b], Yong Wang [c], Enrique Iglesia [a,*]

[a] *Department of Chemical Engineering, University of California at Berkeley, Berkeley, CA 94720, USA*
[b] *ExxonMobil Research and Engineering Company, Corporate Strategic Research, Annandale, NJ 08801, USA*
[c] *Pacific Northwest National Laboratory, Richland, WA 99352, USA*

Received 7 June 2004; revised 5 August 2004; accepted 10 August 2004

Available online 17 September 2004

Abstract

The effects of support identity on catalytic 2-butanol dehydration rates, Brønsted acid site density, and reducibility are examined for WO_x domains supported on ZrO_2, Al_2O_3, SiO_2 (MCM41), and SnO_2. On WO_x–Al_2O_3, 2-butanol dehydration rates (per W atom) increased with increasing WO_x surface density and reached maximum values at WO_x surface densities (9–10 W nm^{-2}) similar to those required for two-dimensional polytungstates, as also found on WO_x–ZrO_2. UV–visible edge energies showed that WO_x domains become larger as WO_x surface density increases. Selective titration of Brønsted acid sites by sterically hindered 2,6-di-*tert*-butylpyridine during 2-butanol dehydration reaction showed that this reaction occurs predominately on Brønsted acid sites for WO_x domains on ZrO_2, Al_2O_3, SiO_2, and SnO_2 supports. Pre-edge features appear in the UV–visible spectra of WO_x–Al_2O_3 samples during 2-butanol dehydration and their intensity increases with WO_x surface density in parallel with measured Brønsted acid site densities and dehydration rates (per W atom). These d–d electronic transitions reflect the formation of reduced centers, consisting of acidic $H^{\delta+}(WO_3)_n{}^{\delta-}$ species, using 2-butanol as a stoichiometric reductant. These processes resemble those on WO_x–ZrO_2, indicating that temporary acid sites generally form from neutral WO_x precursors on all supports. Dehydration turnover rates (per Brønsted acid site) were unaffected by the identity of the support, but for a given WO_x surface density, the number of reduced centers and the density of Brønsted acid sites, but not their intrinsic reactivity, depend on the identity of the support; both reduced centers and Brønsted acid sites are more abundant on ZrO_2-supported than on Al_2O_3-supported samples, as a result of electronic isolation of WO_x domains on the more insulating and unreducible Al_2O_3 supports. The dehydration regioselectivity on Brønsted acid sites is strongly influenced by support, with more electropositive support cations leading to stronger interactions between α-hydrogens in reactants and lattice oxygens, favoring sterically hindered transition states required for the formation of *cis*-2-butene.

Keywords: Tungsten oxide catalysts; Titration by hindered amines; Brønsted acid site density; In situ UV–vis spectroscopy; Support effects

1. Introduction

The ability of porous WO_x–ZrO_2 solids to catalyze alkane isomerization at low temperatures [1] has led to detailed studies of the inorganic structures and reaction pathways responsible for acid catalysis on these materials [2–7]. Some previous studies have shown that Brønsted acid sites form during catalytic reactions from neutral WO_x precursors via reduction of polytungstate structures, which balance the reducibility and accessibility of WO_x domains [8,9]. Spectroscopic and kinetic studies showed that WO_x structure and domain size and the catalytic and electronic properties of these domains depend only on the density of WO_x species on ZrO_2 surfaces [2,8,9]. Raman spectra have detected similar WO_x structures on Al_2O_3 and ZrO_2 supports, which evolve from isolated monotungstates to oligomeric polytungstates with octahedral coordination as WO_x sur-

* Corresponding author.
E-mail address: iglesia@cchem.berkeley.edu (E. Iglesia).

0021-9517/$ – see front matter
doi:10.1016/j.jcat.2004.08.014

face density increases [10]. Monotungstate species on Al_2O_3 catalyze cracking reactions at relatively high temperatures [11,12]; alkene isomerization rates on WO_x–Al_2O_3 catalysts increase with increasing W content [13,14], suggesting that oligomeric WO_x structures are required for selective acid catalysis at low temperatures. WO_x structures supported on SnO_2 catalyze acetonation of sorbose and α-tocopherol synthesis with high rates and selectivity [15], but their properties for other acid-catalyzed reactions remain unexplored. Thus, the reactivity of Brønsted acid sites in WO_x structures, ascribed to specific interactions with ZrO_2 supports in early studies, may well extend to WO_x domains on other oxide supports.

Santiesteban et al. first reported a relation between reducibility and catalytic properties in WO_x–ZrO_2 [7]. Later, UV–vis spectroscopic studies showed that absorption edge energies decreased with increasing WO_x surface density, suggesting a concurrent increase in WO_x domain size [2,8]. These spectroscopic probes also detected the evolution of reduced centers during reduction and catalytic reactions [8,16]. *o*-Xylene isomerization rates increased in parallel with the ability of the materials to chemisorb hydrogen from H_2; both catalytic rates and chemisorption uptakes were proportional to H_2 pressure, as expected from a role of H_2 in forming $H^{\delta+}(WO_3)_n{}^{\delta-}$ with acidic OH groups [8,17,18]. These reduced centers form $H^{\delta+}$ species via H_2 dissociation and require charge delocalization by WO_x domains. 2-Butanol acts as a sacrificial stoichiometric reductant during its catalytic dehydration, thus requiring that Brønsted acid site densities be measured during reaction. These measurements were carried out on WO_x–ZrO_2 catalysts using 2,6-di-*tert*-butylpyridine as a selective titrant of Brønsted acid sites and UV–visible spectroscopy to measure the number and electron-deficient nature of acidic OH groups [16]. On these samples, catalytic dehydration rates were proportional to the number of reduced centers and to the number of Brønsted acid sites, measured by UV–visible spectroscopy and site titrations during reaction, respectively.

Here, we extend these previous catalytic, spectroscopic, and site titration studies to WO_x domains supported on Al_2O_3, SnO_2, and SiO_2 (MCM-41) to examine the effects of supports on the density and the reactivity of active structures. We report the first systematic measurements of acid-catalyzed turnover rates, indicative of the intrinsic reactivity of Brønsted acid sites, on WO_x domains dispersed on various inorganic oxide support materials.

2. Experimental methods

2.1. Catalyst synthesis methods

Detailed synthesis procedures for WO_x–ZrO_2 samples were reported previously [16]. WO_x–Al_2O_3 catalysts were prepared by incipient wetness impregnation of γ-alumina (reforming grade provided by ExxonMobil Corp., 190 $m^2\,g^{-1}$) with aqueous solutions of ammonium metatungstate (Aldrich, reagent grade). Samples were dried in ambient air at 393 K overnight and then treated in ambient air at 723 K for 4 h.

Silica with a MCM-41 structure, one-dimensional pores ($\sim$ 5 nm), and a surface area of 780 $m^2\,g^{-1}$ was prepared using known methods [19,20]. WO_x was anchored on MCM-47 surfaces by controlled hydrolysis of WCl_6. MCM-47 was treated in ambient air at 813 K until only Q^4 lines were detected in its ^{29}Si NMR spectra, indicating the absence of Si–OH groups. This material was dispersed in refluxing toluene, and deionized water was added in stoichiometric amounts required to form a silanol monolayer [21]. WCl_6 (Chemat Technologies, 99.99%) was then added to the refluxing mixture and toluene washes were repeated until WCl_6 was not detected by titration of the effluent with water. These samples were then dried in ambient air at 393 K and treated in flowing dry air at 773 K for 3 h. SnO_2 was prepared by hydrolysis of tin(IV) chloride pentahydrate (98%, Alfa Aesar) with NH_4OH (14.8 N) and treated in dry air at 773 K for 3 h. SnO_2 was impregnated to incipient wetness with aqueous solution of ammonium metatungstate (Stem Chemicals, 99.9%) at 298 K, dried at 383 K, and then treated in flowing dry air at 773 K for 3 h.

The W content, thermal treatment temperatures, and nominal W surface densities are reported in Table 1. Surface densities were estimated from the W content and the BET surface area, measured using a multipoint physisorption isotherm for N_2 at its normal boiling point. The nomenclature used throughout (e.g., W(9.8)Al) lists the surface

Table 1
Tungsten content, thermal treatment, WO_x surface density, and notation used for all samples in this study

W concentration (wt% WO_3)	Treatment temperature (K)	Nominal surface density[a] ($W\,nm^{-2}$)	Nomenclature
5	723	1.1	W(1.1)Al
10	723	2.1	W(2.1)Al
20	723	4.3	W(4.3)Al
27	723	5.8	W(5.8)Al
35	723	7.6	W(7.6)Al
45	723	9.8	W(9.8)Al
60	723	13.0	W(13.0)Al
50	773	6.5	W(6.5)Si
67	773	23.2	W(23.2)Si
26	773	7.7	W(7.7)Sn
30	773	3.9	W(3.9)Zr
30	873	5.4	W(5.4)Zr
30	923	6.8	W(6.8)Zr
30	973	9.6	W(9.6)Zr
30	1023	14.8	W(14.8)Zr
30	1073	17.2	W(17.2)Zr
15	873	2.9	W(2.9)Zr
15	1023	7.9	W(7.9)Zr
15	1073	10.5	W(10.5)Zr
15	1123	13.5	W(13.5)Zr
15	1173	29.8	W(29.8)Zr

[a] Estimated from nominal W content and BET surface area of samples after indicated thermal treatment.

density in parentheses (as W nm^{-2}) and the support cation immediately thereafter.

2.2. Catalytic reactions of 2-butanol

Catalytic 2-butanol dehydration rates and alkene selectivities were measured at 373 K in a quartz flow reactor (1.0 cm i.d.) using samples (0.027–0.250 g) dispersed on a quartz frit. All samples were treated in flowing dry air (0.83 cm^3 s^{-1}) at 723 K for WO_x–Al_2O_3 (WAl), WO_x–SiO_2 (WSi), at 773 K for WO_x–ZrO_2 (WZr), and at 673 K for WO_x–SnO_2 (WSn) for 1 h before catalytic measurements. Liquid 2-butanol (Aldrich, 99.5%, anhydrous) was vaporized into flowing He (Airgas, ultrahigh purity grade) at 100.1 kPa and 373 K by controlled injection with a syringe pump to give a constant 2-butanol pressure (0.5 kPa). Reactant conversion was varied by changing the He flow rate (0.3–4.85 cm^3 s^{-1} for WAl, WSi, and WSn and 0.15–5.78 cm^3 s^{-1} for WZr) at constant 2-butanol pressure (0.5 kPa). Reactant and product concentrations were measured by gas chromatography (Hewlett-Packard 6890 GC, 30 m HP-1 methyl silicone capillary column, flame ionization detector). 2-Butanol dehydration rates are reported per W atom and as turnover rates per Brønsted acid site, estimated by site titrations during reaction.

2.3. Titration of acid sites during 2-butanol dehydration catalysis

Liquid mixtures of 2-butanol with pyridine (Fischer, 99.9%) or 2,6-di-*tert*-butylpyridine (Aldrich, 97%) were prepared using 2-butanol (4.5 ml; Aldrich, 99.5%, anhydrous) and 10–20 μl of either organic base. The resulting titrant–reactant mixture was introduced into a He stream (1.33 cm^3 s^{-1}) at a liquid volumetric flow rate of 0.09 cm^3 h^{-1}, resulting in mixtures containing 0.5 kPa 2-butanol, 1.25–2.5 Pa pyridine, or 0.45–0.90 Pa 2,6-di-*tert*-butylpyridine. The amount of titrant adsorbed on the catalyst was calculated from its concentration in the effluent, measured by gas chromatography, using the same chromatographic protocols as for 2-butanol dehydration.

2.4. In situ ultraviolet–visible diffuse reflectance spectroscopy

Diffuse reflectance electronic spectra were measured in the UV–vis range using a Varian (Cary 4) spectrometer with a Harrick Scientific diffuse reflectance attachment (DRP-XXX) and a controlled environment chamber (DRA-2CR). Reflectance measurements were converted into pseudo-absorbance units ($F(R_\infty)$) using the Kubelka–Munk formalism and MgO as a standard reflector [22]. Samples were dehydrated in flowing dry air at 723 K, cooled in air to 298 K, and treated in He at 298 K before measuring spectra at 723 K in flowing dry air. Absorption edge energies were estimated from the x intercept of a linear fit of the near edge region plotted as $(F(R_\infty)h\nu)^{1/2}$ vs $h\nu$ [8]. UV–vis spectra were also recorded on similarly treated samples during steady-state 2-butanol dehydration (0.5 kPa 2-butanol, He (1.33 cm^3 s^{-1})) at 423 K (WAl) and 323 K (WZr).

3. Results and discussion

3.1. Catalytic dehydration of 2-butanol

2-Butanol dehydration was used to probe acid properties and in situ formation of Brønsted acid sites in WAl, WSi, and WSn samples with varying W surface densities. Only monomolecular dehydration products (1-butene, *cis*- and *trans*-2-butenes) formed; ether products of bimolecular reactions were not detected. 2-Butanol dehydration rates decreased with increasing reactant conversion, varied by changing residence time, on WAl (Fig. 1), WSi, and WSn, as also found earlier on WZr [16]; these effects reflect competitive adsorption of the H_2O formed during reaction [16]. Reaction rates were obtained by extrapolation to zero 2-butanol conversion, using a rate expression (Eq. (1); [16]) containing two constants k' and α

$$r = \frac{\left(\frac{k_2[L]}{1+k_2/k_3}\right)}{\left(1+\frac{k_{-3}(k_{-1}+k_2)}{k_3k_1(1+k_2/k_3)}\frac{[H_2O]}{[A]}\right)} = \frac{k'}{1+\alpha\frac{[H_2O]}{[A]}}, \quad (1)$$

where $[H_2O]$ is the water pressure, $[A]$ is the 2-butanol pressure, and $[L]$ is the total concentration of active sites; kinetic

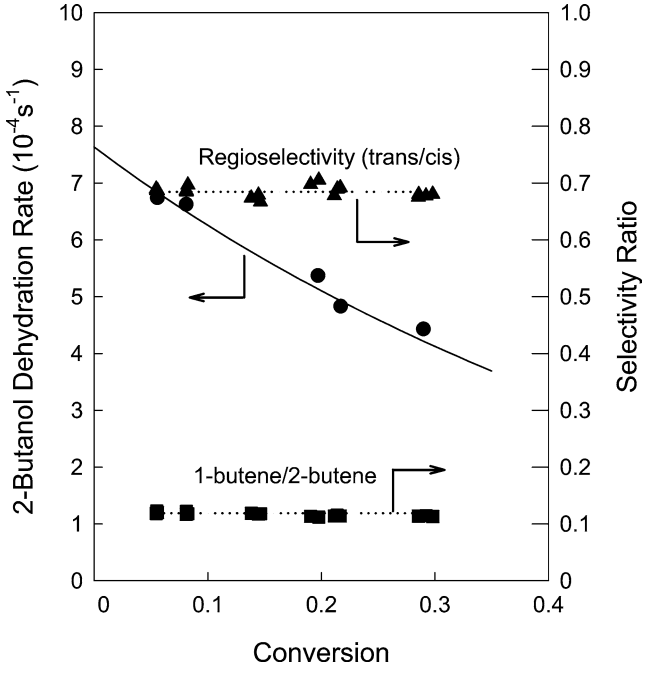

Fig. 1. 2-Butanol dehydration rate (per W atom) and selectivity ratios at 373 K as a function of conversion for W(9.8)Al [0.5 kPa 2-butanol, 100.8 kPa He, 5–34 mol 2-butanol/(g-atom W h)]. ● Represents average conversion and rate values at a certain space velocity; — calculated rate using Eq. (1) as a function of conversion.

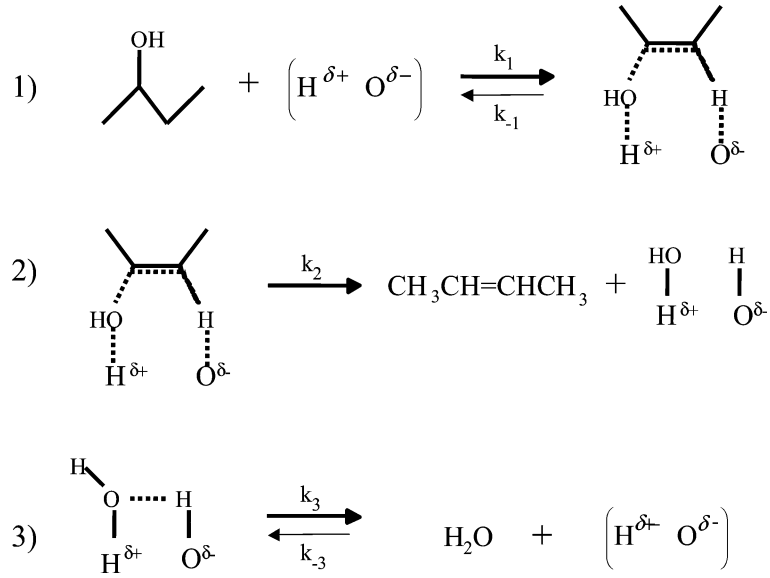

Scheme 1. Proposed elementary steps for 2-butanol dehydration on supported WO_x catalysts.

constants were obtained from residence time reaction rate data using nonlinear regression methods.

The mechanism for 2-butanol dehydration (Scheme 1; [16]) includes the reversible associative adsorption of 2-butanol on conjugate acid–base pairs via concerted interactions of OH groups and a β-hydrogen in 2-butanol with this site pair (step 1). This step is followed by irreversible bimolecular (E2) decomposition of adsorbed butanol to butene isomers, leaving two vicinal OH groups (step 2). The catalytic cycle is completed by reversible recombination of OH groups to form H_2O, which desorbs to restore Brønsted acid sites (step 3). Eq. (1) was derived from these steps and confirmed by kinetic data on WZr [16]; we note that k' in Eq. (1) is the zero-order 2-butanol dehydration rate obtained by extrapolation of rate data to zero reactant conversion.

The extent of reactant conversion did not influence alkene selectivity on any catalyst (e.g. Fig. 1, W(9.8)Al). This indicates that alkenes do not readsorb and isomerize during 2-butanol dehydration, apparently because active sites are saturated with butanol-derived intermediates, as shown by the observed zero-order kinetic dependence on 2-butanol reactant pressure [16]. Thus, observed selectivities reflect primary reactions of butanol-derived intermediates. Fig. 2 shows *trans*/*cis* 2-butene and 1-butene/2-butene selectivity ratios for representative catalysts on each support. *Trans*/*cis* ratios, denoted herein as regioselectivity ratios, are higher on WAl, WSi, and WSn than on WZr (e.g., 0.9 (WSi) and 0.4 (WZr)), but even on the first three samples, they are below equilibrium values (2.5 at 373 K [16]). On WAl, regioselectivity ratios increased with decreasing WO_x surface density, but did not depend on surface density for WZr and WSi. 1-Butene/2-butene ratios were similar on all supports and independent of WO_x surface density. This dependence of regioselectivity ratios on supports and, for WAl, on surface density, will be discussed later, after examining the number and type of acid sites responsible for these catalytic dehydration reactions.

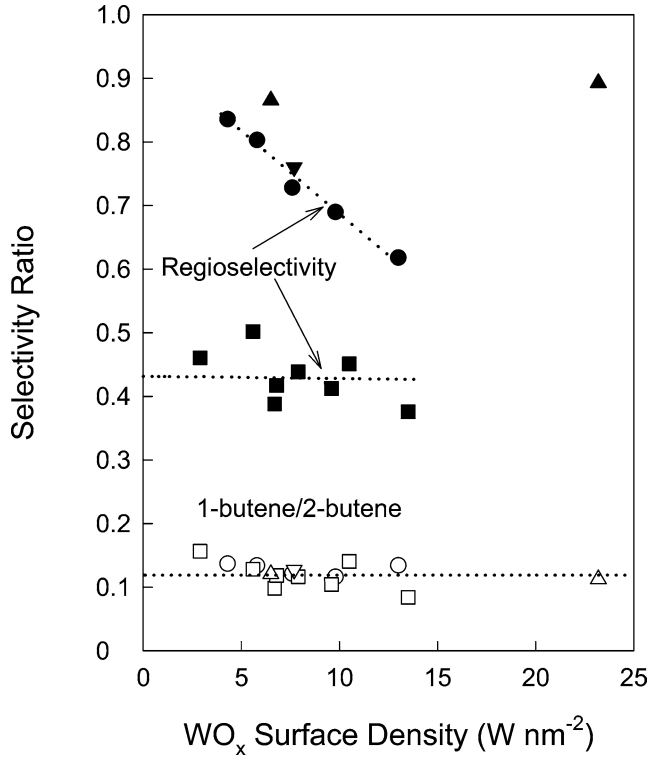

Fig. 2. Selectivity ratios at 373 K as a function of WO_x surface density at ∼ 5% conversion [0.5 kPa 2-butanol, 100.8 kPa He]. Different ratios and catalysts are shown: regioselectivity ratio of WAl (●), 1-butene/2-butene ratio of WAl (○), regioselectivity ratio of WZr (■), 1-butene/2-butene ratio of WZr (□), regioselectivity ratio of WSi (▲), 1-butene/2-butene ratio of WSi (△), regioselectivity ratio of WSn (▼), 1-butene/2-butene ratio of WSn (▽).

Next, we examine the effects of support and WO_x surface density on 2-butanol dehydration rates for WAl, WZr,

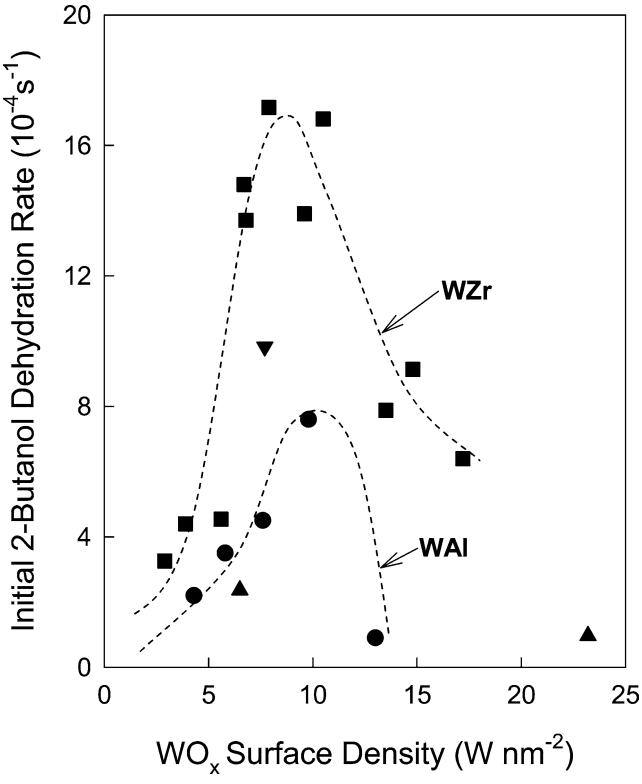

Fig. 3. Initial 2-butanol dehydration rates (per W atom) at 373 K as a function of WO_x surface density [0.5 kPa 2-butanol, 100.8 kPa He]. Different catalysts are shown: WAl (●), WZr (■), WSi (▲), and WSn (▼).

WSi, and WSn (Fig. 3). Dehydration rates (per W atom) on WAl are lower than on WZr at all WO_x surface densities; they show a maximum value at WO_x surface densities (9–10 W nm^{-2}) slightly above a theoretical polytungstate monolayer, as also found on WZr at slightly lower surface densities (∼ 8 W nm^{-2}) [16]. WSi catalysts show lower dehydration rates (per W atom) than WAl samples, while dehydration rates on WSn are intermediate between those measured on WZr and WAl (Fig. 3).

Dehydration rates per W atom reflect the combined effects of the dispersion of WO_x domains and of the reactivity of Lewis and Brønsted acid sites coexisting in these samples. Their relative importance is difficult to discern, among other reasons, because Brønsted acid sites form by reduction of WO_x centers with H_2 or 2-butanol during catalytic reactions [8,9,16,18]. Site titrations with hindered organic bases *during* catalysis showed that rates on WZr depend only on the number of Brønsted acid sites [7,16]. Stoichiometric reductants, such as H_2 during *o*-xylene isomerization [9,18] and 2-butanol during its dehydration [16], form active $H^{\delta+}(WO_3)_n{}^{\delta-}$ centers. Their density depends on the availability and reactivity of the reductant and on the ability of accessible WO_x centers to stabilize the active $H^{\delta+}$ species by delocalizing the balancing negative charge [8,9,16]. The latter depends on the reducibility of WO_x domains, which increases as the size of these domains increases on ZrO_2 supports [8,16], but which can also depend on the chemical identity of the support on which these domains are dispersed.

3.2. Selective titration of Brønsted and Lewis acid sites during 2-butanol dehydration

Here, we probe the effects of support and surface density on the density of Brønsted acid sites ($H^{\delta+}(WO_3)_n{}^{\delta-}$) measured by site titration methods and on the number of reduced centers detected by in situ UV–visible spectroscopy during dehydration catalysis. Then, we use these site densities to report turnover rates (per Brønsted acid site) on WO_x domains supported on ZrO_2, Al_2O_3, SiO_2, and SnO_2.

Titration methods can be used to measure the number of acid sites during catalytic reactions, as well as the respective catalytic involvement of Brønsted and Lewis acid sites. Sterically hindered pyridines titrate Brønsted acid sites selectively because their N atoms cannot coordinate to Lewis acid centers, as shown by Brown and Johanneson [23] and later by others [7,11,16,24,25]; in contrast, pyridine titrates both types of acid sites via protonation or coordination. Pyridine and 2,6-di-*tert*-butylpyridine are used here to determine the involvement and reactivity of Brønsted and Lewis acid centers in 2-butanol dehydration. On WZr and WO_x-based polyoxometalate clusters, 2-butanol dehydration occurs predominately on Brønsted acid sites [16]. 2,6-Di-*tert*-butylpyridine addition did not influence 2-butanol dehydration on γ-Al_2O_3, on which only Lewis acid sites exist, but suppressed dehydration catalysis on WZr and polyoxometalate catalysts [16].

Figs. 4–6 show dehydration rates as a function of cumulative titrant adsorption on W(5.8)Al, W(6.5)Si, and W(7.7)Sn. The leftmost section in each figure shows time-on-stream behavior before the titrant is added, while the rest shows rates as a function of the amount of titrant adsorbed, measured at constant intervals as titrant was continuously added. Data points become more closely spaced as acid sites become saturated with the titrant. Catalysts titrated with 2,6-di-*tert*-butylpyridine maintain some residual activity, even after saturation (Figs. 4–6), reflecting minor dehydration contributions from Lewis acid sites, which do not interact with 2,6-di-*tert*-butylpyridine.

Titration with 2,6-di-*tert*-butylpyridine led to a linear decrease in dehydration rates with increasing adsorbed titrant, consistent with stoichiometric titration of active sites. The linear nature of this decrease in rate does not unequivocally reflect the presence of sites uniform in catalytic behavior, because strong binding leads to sequential titration of all acid sites along the catalyst bed, irrespective of their reactivity. The small residual rates observed after saturation with 2,6-di-*tert*-butylpyridine were similar on WAl and WSi, but three times higher on WSn (Table 2). On WAl, they remained constant as surface density increased, but ultimately decreased as WO_3 clusters formed at surface densities above 10 W nm^{-2}. Residual dehydration rates after 2,6-di-*tert*-butylpyridine saturation may reflect exposed W^{6+} cations

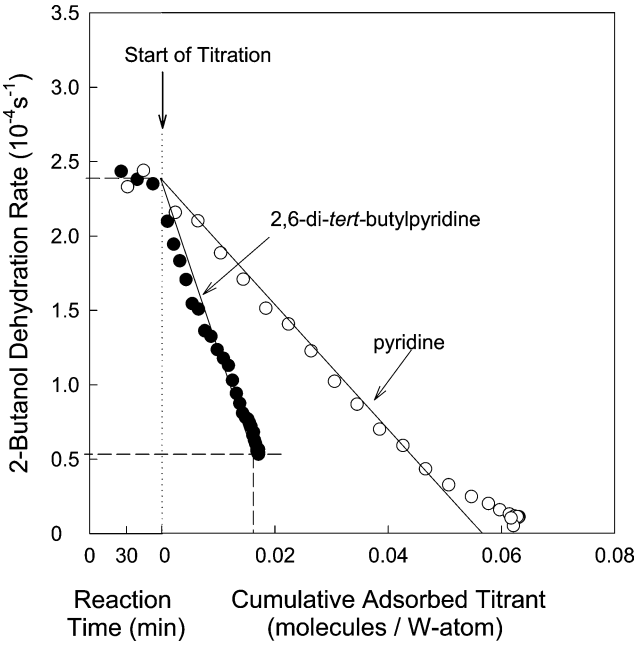

Fig. 4. Titration of acid sites on W(5.8)Al during 2-butanol dehydration. Reaction rates (per W atom) at 373 K as a function of the cumulative amount of titrant (2,6-di-*tert*-butylpyridine or pyridine) adsorbed during reaction [0.5 kPa 2-butanol, 100.1 kPa He, 1.625 Pa pyridine, 0.45 Pa 2,6-di-*tert*-butylpyridine].

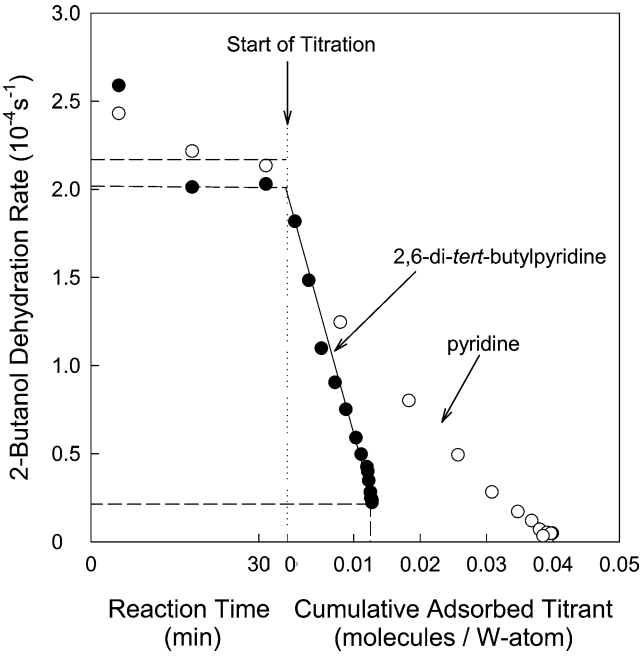

Fig. 5. Titration of acid sites on W(6.5)Si during 2-butanol dehydration. Reaction rates (per W atom) at 373 K as a function of the cumulative amount of titrant (2,6-di-*tert*-butylpyridine or pyridine) adsorbed during reaction [0.5 kPa 2-butanol, 100.1 kPa He, 2.5 Pa pyridine, 0.45 Pa 2,6-di-*tert*-butylpyridine].

acting as Lewis centers, the dispersion of which ultimately decreases at high surface densities. These data together with the negligible dehydration rates on Lewis acid sites present in pure γ-Al_2O_3 [16] and with the similar residual rates measured on WSi (Table 2), even though silica lacks Lewis acid sites, suggest that sites on support surfaces are not responsible for these residual rates after 2,6-di-*tert*-butylpyridine saturation.

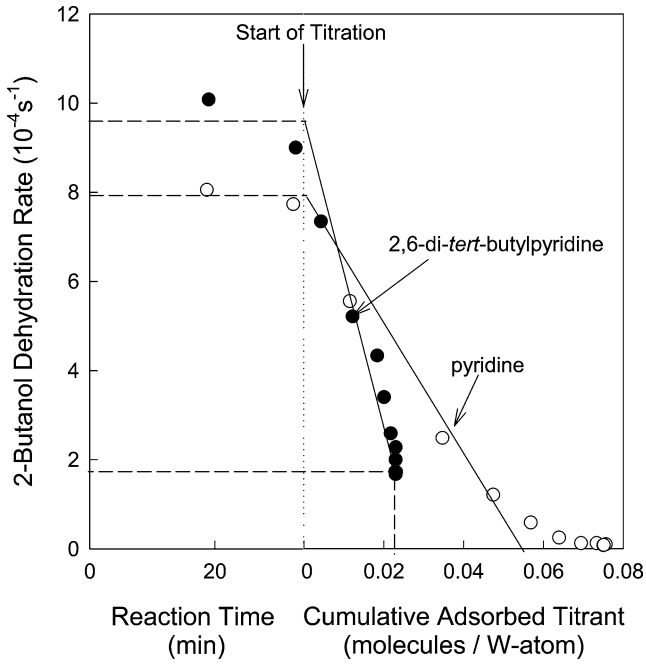

Fig. 6. Titration of acid sites on W(7.7)Sn during 2-butanol dehydration. Reaction rates (per W atom) at 373 K as a function of the cumulative amount of titrant (2,6-di-*tert*-butylpyridine or pyridine) adsorbed during reaction [0.5 kPa 2-butanol, 100.1 kPa He, 2.5 Pa pyridine, 0.74 Pa 2,6-di-*tert*-butylpyridine].

Table 2
Comparison of residual 2-butanol dehydration rates on WAl, WSi, and WSn

Catalyst	Residual dehydration rate[a] (10^{-4} s^{-1})
W(4.3)Al	0.44
W(5.8)Al	0.54
W(7.6)Al	0.41
W(9.8)Al	0.50
W(13.0)Al	0.08
W(6.5)Si	0.24
W(23.2)Si	0.18
W(7.7)Sn	1.70

[a] Determined from residual 2-butanol dehydration at 373 K after saturation with 2,6-di-*tert*-butylpyridine (per W atom).

Titrant uptakes are greater for pyridine than for 2,6-di-*tert*-butylpyridine, because pyridine saturates both Lewis and Brønsted acid sites before titrating downstream active Brønsted acid sites involved in dehydration reactions. Pyridine titration suppressed 2-butanol dehydration activity almost completely (Figs. 4–6), suggesting that Lewis acid sites are responsible for the residual rates measured after 2,6-di-*tert*-butylpyridine saturation; the number of Lewis acid sites is given by the difference between the amounts of 2,6-di-*tert*-butylpyridine and pyridine required to saturate each sample. For example, the density of Brønsted acid sites on W(5.8)Al (Fig. 4) was 0.017 sites/W atom, while the to-

tal number of acid sites, obtained by extrapolating the initial slope of dehydration rate as a function of the cumulative pyridine adsorbed to zero, was 0.058 sites/W atom; their difference (0.041 sites/W atom) reflects the number of Lewis acid sites, whether they reside on Al_2O_3 and are catalytically inactive at 373 K, or on WO_x domains and contribute to residual rates after saturation with 2,6-di-*tert*-butylpyridine. On this sample, the apparent turnover rate for Lewis acid catalysis is given by the residual rate divided by the number of Lewis acid sites. This apparent turnover rate ($\sim 1.3 \times 10^{-3}$ s^{-1}) is much lower than on Brønsted acid sites ($\sim 17.4 \times 10^{-3}$ s^{-1}); the latter was obtained by dividing the part of the initial dehydration rate influenced by 2,6-di-*tert*-butylpyridine by the number of titrant molecules required to suppress dehydration rates.

Fig. 7 shows Brønsted (a) and Lewis (b) acid site densities in WAl, WZr, WSi, and WSn samples with different surface densities. The WAl sample with 9.8 W nm^{-2} shows the highest Brønsted acid site density (per W atom) and also the highest 2-butanol dehydration rate (per W atom) (Fig. 3) on Al_2O_3 supports. This site density corresponds to one $H^{\delta+}$ per 35 W atoms, indicating that effective charge delocalization requires significant spatial isolation of reduced centers as they form during reaction. Lewis acid site densities on WAl (Fig. 7b) are highest (~ 0.051 sites/W atom) at low WO_x surface densities (4.3 W nm^{-2}). Brønsted acid site densities on W(7.7)Sn are similar to those on WAl samples with similar WO_x surface densities and lower on WSi. WZr samples show higher Brønsted acid site densities than WO_x species on other supports at all WO_x surface densities; they also show higher 2-butanol dehydration rates per W atom (Fig. 3). Lewis acid site densities (per W atom) on WAl and WZr decrease as WO_x surface densities approach theoretical polytungstate monolayer values (~ 8 W nm^{-2}) (Fig. 7b), apparently because the accessibility of W^{6+} cations decreases as three-dimensional WO_3 clusters form. At low WO_x surface densities, Al_2O_3-supported samples contain significant exposed support surfaces, which can contribute to measured Lewis acid site densities but not to measured catalytic rates, because of the negligible catalytic reactivity of exposed Al_2O_3 surfaces [16].

The ratio of initial to residual dehydration rates during 2,6-di-*tert*-butylpyridine titration indicates that surface density effects on regioselectivity for WAl samples may reflect parallel dehydration pathways on Lewis acid sites, which become less prevalent as WO_x surface density increases. These sites, which are not titrated by 2,6-di-*tert*-butylpyridine, give rise to the higher residual regioselectivity ratio observed after saturation with this titrant (*trans*/*cis* = 0.88) compared with that measured before the titrant is introduced (*trans*/*cis* = 0.68–0.84 (Fig. 8)), apparently because of differences in regioselectivity between Brønsted and Lewis acid sites. Contributions from dehydration turnovers on Lewis acid sites appear to be responsible for the observed regioselectivity changes with WO_x density on WAl. In contrast with WAl, WZr and WSi give similar initial and residual regioselectivity ratios; slightly different ratios were obtained on WSn. Different regioselectivities on Brønsted and Lewis acid sites may well account for the changes of regioselectivity with WO_x surface density, but not for the different regioselectivities found for different supports (Fig. 2). Below, we discuss how supports can influence regioselectivity.

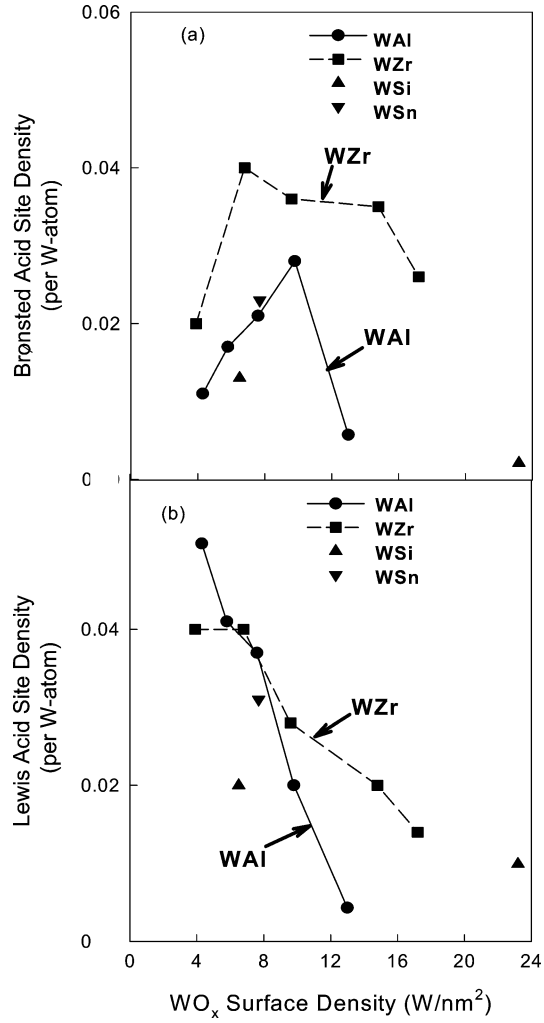

Fig. 7. Brønsted (a) and Lewis (b) acid site densities as a function of WO_x surface density. Acid site densities were determined by titration during 2-butanol reaction at 373 K with pyridine (Brønsted + Lewis acid site density) or 2,6-di-*tert*-butylpyridine (Brønsted acid site density). Catalysts shown: WAl (●), WZr (■), WSi (▲), and WSn (▼).

A kinetic preference for *cis*-alkenes is typical of E2 elimination dehydration pathways [26–28], for which the basicity of lattice oxygen anions controls regioselectivity [28]. More basic lattice oxygens favor interactions with the α-hydrogen, as depicted in Scheme 2a. Thus, electron density at the α-C atom increases, which favors OH abstraction from adsorbed butanol. This interaction stabilizes transition states leading to *cis*-alkenes (Scheme 2a). More basic oxygen anions and the stronger interactions that ensue compensate for steric strain in the eclipsed conformation required for *cis*-selectivity (Scheme 2a), which would otherwise be much

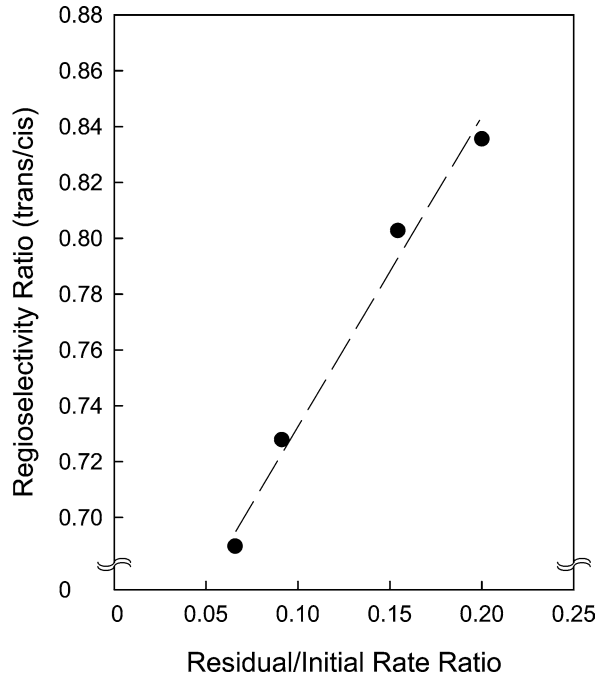

Fig. 8. Initial regioselectivity ratio on WAl samples at 373 K as a function of residual/initial rate ratio. [0.5 kPa 2-butanol, 100.1 kPa He, 1.625 Pa pyridine, 0.45 Pa 2,6-di-*tert*-butylpyridine].

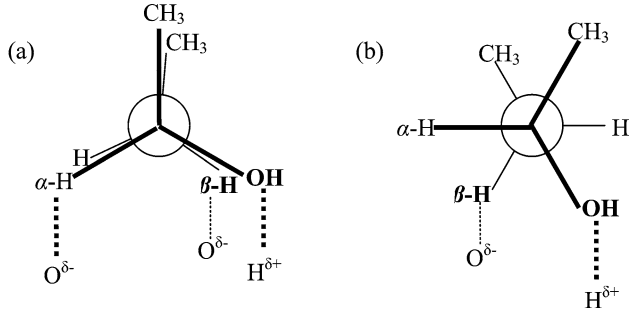

Scheme 2. E2 dehydration transition states required for the formation of *cis*-alkenes (a) and *trans*-alkenes (b). The additional interaction of the lattice oxygen (electron pair donor) with the α-hydrogen (a) is likely to be responsible for the preference of the formation of *cis*-alkenes, although the eclipsed conformation in transition state (a) is energetically less favorable.

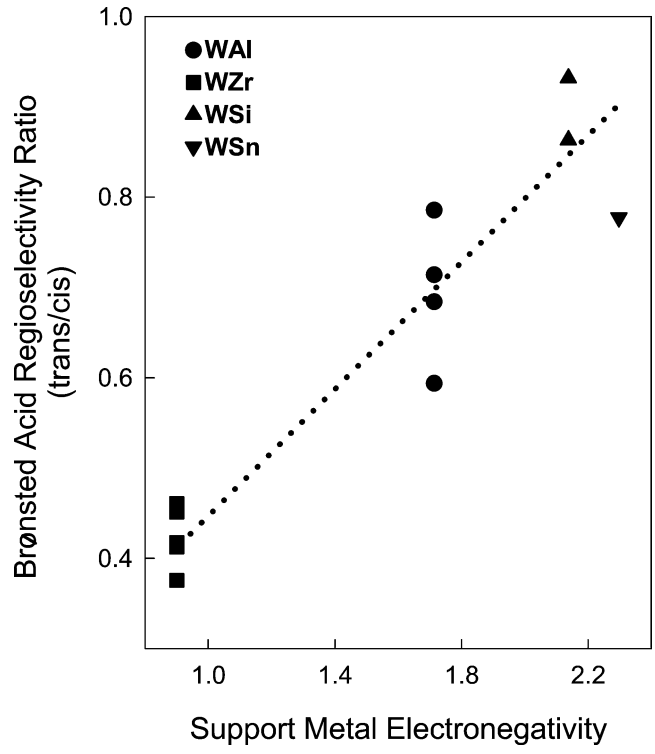

Fig. 9. Brønsted acid regioselectivity ratios at 373 K as a function of Sanderson electronegativity of the metal in the oxide support. Catalysts shown: WAl (●), WZr (■), WSi (▲), and WSn (▼). For WZr and WSi Brønsted regioselectivity equals overall regioselectivity (OR), for WAl and WSn it had been calculated taking into account the different selectivities on Lewis acid sites as obtained by 2,6-di-*tert*-butylpyridine titration (see Appendix). [0.5 kPa 2-butanol, 100.1 kPa He, 0.45 (WAl), 0.9 (WZr), 0.45 WSi) and 0.74 Pa 2,6-di-*tert*-butylpyridine (WSn).]

less stable than the staggered conformation (Scheme 2b) involved in *trans*-alkene formation. These interactions may be regarded as inductive effects that increase electron density on the α-C atom.

2-Butanol dehydration on γ-Al_2O_3, $MgAl_2O_4$, $AlPO_4$, $Ba_3(PO_4)_2$, $Ca_3(PO_4)_2$, and $CaHPO_4$ Lewis acid catalysts show lower regioselectivity ratios with increasing oxide basicity [28]. The intimate contact between WO_x domains and the support in well-dispersed structures leads to electron transfer mediated by bridging oxygens, the basicity of which increases as the electron withdrawing tendency of support cations decreases. Thus, less acidic support cations would lead to more basic oxygens and to a preference for *cis*-alkenes in E2 elimination reactions, as indeed found when regioselectivity ratios are related to the electronegativity of these cations. Fig. 9 shows Brønsted acid regioselectivity ratios as a function of support cation electronegativity for supported WO_x catalysts. The Brønsted acid regioselectivity ratio is calculated from the overall catalyst regioselectivity ratio taking into account the different selectivities on Lewis acid sites obtained for WAl (Appendix). On each support, the regioselectivity on Brønsted acid sites is independent of WO_x surface density and increases with the Sanderson electronegativity [29] of the support cation (Fig. 9).

Titration of Brønsted acid sites with 2,6-di-*tert*-butylpyridine during 2-butanol dehydration was carried out at two temperatures (373 and 403 K) on WAl(5.8) to probe the in situ formation of Brønsted acid sites. Brønsted acid site densities increased from 0.017 to 0.026 sites/W atom as the reaction temperature increased from 373 to 403 K (Fig. 10). These findings cannot be reconciled with the catalytic involvement of permanent acid sites, the number of which cannot be influenced by reaction temperature. These data reflect instead the effects of temperature on the extent of reduction of WO_x domains, which lead in turn to an increase in the number of Brønsted acid sites. The observed strong temperature dependence of 2-butanol dehydration rates therefore reflects both the activation energy for E2 elimination path-

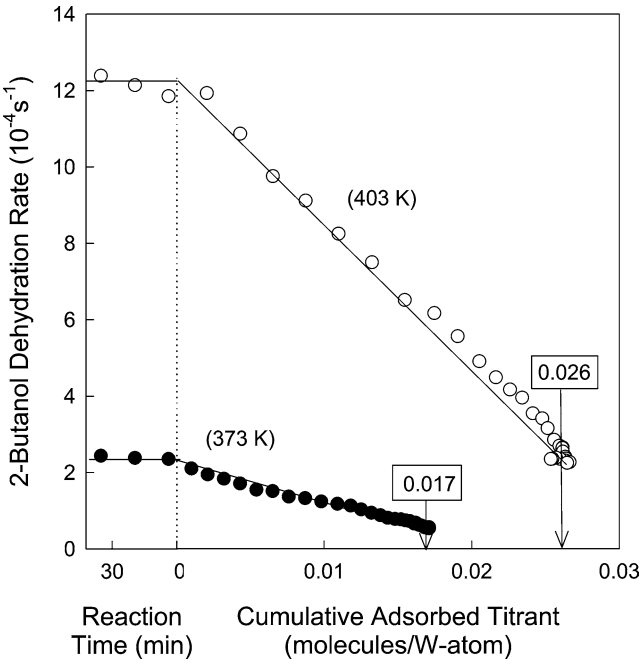

Fig. 10. Titration of acid sites on W(5.8)Al with 2,6-di-*tert*-butylpyridine during 2-butanol dehydration. Reaction rates at 373 K and 403 K (per W atom) as a function of the cumulative amount of 2,6-di-*tert*-butylpyridine adsorbed during reaction [0.5 kPa 2-butanol, 100.1 kPa He, 0.45 Pa 2,6-di-*tert*-butylpyridine (373 K), 0.9 Pa 2,6-di-*tert*-butylpyridine (403 K)].

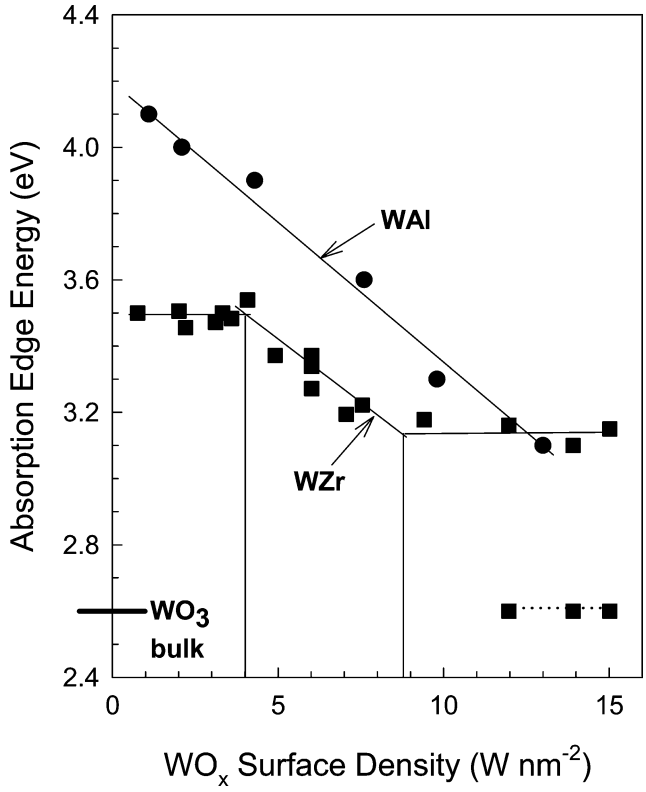

Fig. 11. Absorption edge energies as a function of WO_x surface density. Catalysts shown: WAl (●) and WZr (■).

ways and an increase in the number of Brønsted acid sites with increasing temperature.

These data show the predominant contributions of Brønsted acid sites to measured 2-butanol dehydration rates on WAl, WSi, and WSn. Even for the sample with lowest surface density (W(4.3)Al), Brønsted acid sites contribute more than 70% of measured dehydration rates. Previous studies have shown that these Brønsted acid sites form on polytungstate domains supported on ZrO_2 during reactions of 2-butanol [16] or H_2/*o*-xylene [18] reactants via reduction processes leading to $H^{\delta+}(WO_3)_n{}^{\delta-}$ reduced centers detected by UV–visible spectroscopy and titrated by hindered pyridine bases. Next, we extend these spectroscopic studies to show that similar in situ reduction processes lead to the observed catalytic behavior of WO_x domains supported on Al_2O_3; these measurements are also used to probe the effects of supports on the electronic properties of WO_x species by comparing spectra of WAl with those reported for WZr [8,16].

3.3. UV–vis spectroscopy studies—Nature of active sites

On WZr, absorption edge energies decreased with increasing WO_x surface density, because charge delocalization becomes more effective on WO_x domains of larger size [2,8]. More effective charge delocalization leads to more reducible domains, because reduction introduces additional electron density. The size of semiconductor domains, their reducibility, and their catalytic reactivity are connected by this requirement for charge delocalization for many oxide systems [30]. The formation of reduced centers is detected in UV–visible spectra by the appearance of absorption features in the spectral region below the edge; these features reflect d–d electronic transitions that become possible upon reduction of W^{6+} to W^{6-x} centers during 2-butanol reactions on WZr [16] or during reduction in H_2 [8]. Their intensity increased in parallel with the ability of the materials to catalyze dehydration and isomerization reactions.

The absorption edge reflects the energy required for promoting an electron from the highest occupied orbital (HOMO) or valence band to the lowest unoccupied orbital (LUMO) or conduction band. In WO_x, relevant electron transfer occurs from O atoms to W centers and the photon energies required depend on local coordination, domain size [31,32], and support [31]. Fig. 11 shows absorption edge energies for WAl and WZr as a function of WO_x surface density. WZr showed three distinct regions. At low surface densities (< 3 W nm^{-2}), the edge remained constant (~ 3.49 eV), as expected for isolated species, and then decreased as surface density increased (4–8 W nm^{-2}) because of the growth of two-dimensional polytungstate domains. A polytungstate monolayer (with an edge energy of 3.2 eV) coexists at even higher surface densities with three-dimensional structures with edge energies (~ 2.6 eV) typical of bulk WO_3 crystallites. In contrast, WAl samples show a gradual decrease in edge energy with increasing WO_x sur-

face density and higher edge energies for isolated species than on ZrO_2 (3.9–4.1 eV vs 3.4 eV for 1.1–3.9 W nm^{-2}).

These data suggest that WO_x structures evolve less uniformly on Al_2O_3 than on ZrO_2, and that more insulating Al_2O_3 supports (relative to ZrO_2; 8.7 eV vs 5.0 eV (UV–vis absorption edge of the respective support material) [33]) lead to weaker electron transfer between WO_x and the support, to greater electronic isolation of small WO_x domains, and to less reducible WO_x species. Thus, electron delocalization beyond WO_x domains, as electron density increases during reduction, requires higher activation energies on Al_2O_3 than on ZrO_2 supports. This leads to the higher edge energies measured for isolated monotungstate species on Al_2O_3 compared with similar structures on ZrO_2; these electronic differences also reflect the tetrahedral coordination of W centers on Al_2O_3 at low WO_x surface densities [34], which differs from the distorted octahedral symmetry characteristic of isolated monotungstate species on ZrO_2 [8]. X-ray absorption near-edge spectra showed that WO_x domains on Al_2O_3 exhibit octahedral coordination at surface densities required for polytungstate monolayers (~ 8 W nm^{-2}) [34]. The data in Fig. 11 indicate that the effective size of WO_x domains increased with increasing WO_x surface density on both ZrO_2 and Al_2O_3. The resulting ability of larger domains to delocalize charge, required for low-energy electron transitions and also for chemical reduction, increased with WO_x surface density on both supports, but greater electronic isolation on Al_2O_3 surfaces renders WO_x domains less reducible than those on ZrO_2 for a given WO_x surface density.

WZr forms active $H^{\delta+}(WO_3)_n{}^{\delta-}$ Brønsted acid sites during dehydration reactions [16]; these reduction processes lead to pre-edge features in UV–visible spectra. Fig. 12 shows UV–vis spectra during steady-state 2-butanol dehydration at 423 K (WAl; Fig. 12b) and 323 K (WZr; Fig. 12a) for samples with similar WO_x surface densities. Higher temperatures are required to detect reduced centers on WAl than on more active WZr, preventing quantitative reducibility comparisons but indicating a clear relation between catalytic rates and reduction properties for WO_x domains. WAl samples showed weaker molecule-like absorption features than WZr, and they appeared at higher absorption energy (2.9 vs 2.2 eV); these effects appear to reflect the less uniform nature of Al_2O_3-supported samples, confirmed by their monotonic decrease in edge energy with increasing surface density (Fig. 11), as well as the more insulating nature of the Al_2O_3 support, which causes the photon energies required for electronic transitions to also increase for the O-to-W electron transfer processes responsible for absorption at the edge. At higher surface densities (> 10 W nm^{-2}), preedge absorption intensities become similar on the two supports, as O removal from WO_x clusters becomes the predominant mechanism for reduction and WO_x domains grow and become less intimately connected to support surfaces [16].

Fig. 13 shows integrated UV–vis intensities in the preedge region (2.0–3.4 eV (WAl), 1.5–3.2 eV (WZr)) for WAl (423 K) and WZr (323 K) samples with varying surface

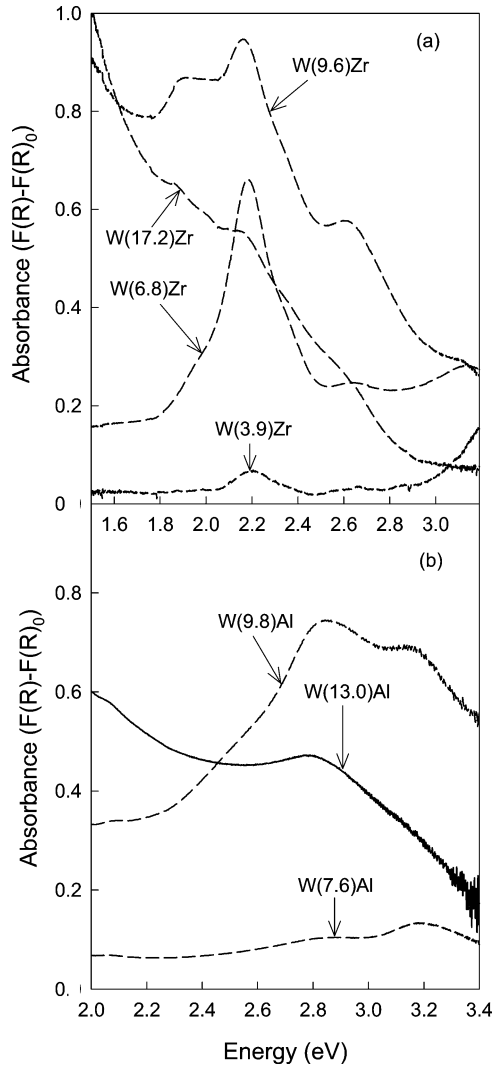

Fig. 12. UV–vis Kubelka–Munk absorption intensity in the preedge (visible) region as a function of WO_x surface density for WZr (a) and WAl (b) during steady-state dehydration catalysis (after 1 h) with 2-butanol (0.5 kPa) at 323 K (WZr, (a)) and 423 K (WAl, (b)). $F(R)_0$ designates the Kubelka–Munk absorption in the absence of 2-butanol.

density. These data reflect the number of electrons introduced into WO_x domains upon reduction, either by forming $H^{\delta+}(WO_3)_n{}^{\delta-}$ or oxygen-deficient WO_{3-x} species. The number of reduced centers increased with increasing surface density on WAl and WZr and ultimately decreased as W species reside predominately at inaccessible positions within three-dimensional crystallites. The maximum number of reduced centers (per W atom) was measured on both supports at WO_x surface densities similar to those required for maximum Brønsted acid site densities (Fig. 7a) and 2-butanol dehydration rates (per W atom; Fig. 3). At even higher surface densities, preedge absorption intensities (Fig. 13) do not correlate with acid site density (Fig. 7a) or dehydration rates (Fig. 3), because reduction processes involving O removal and leading to inactive reduced centers become prevalent as WO_x clusters form; these O-deficient centers absorb photons in the preedge region but cannot reduce further to form O–H

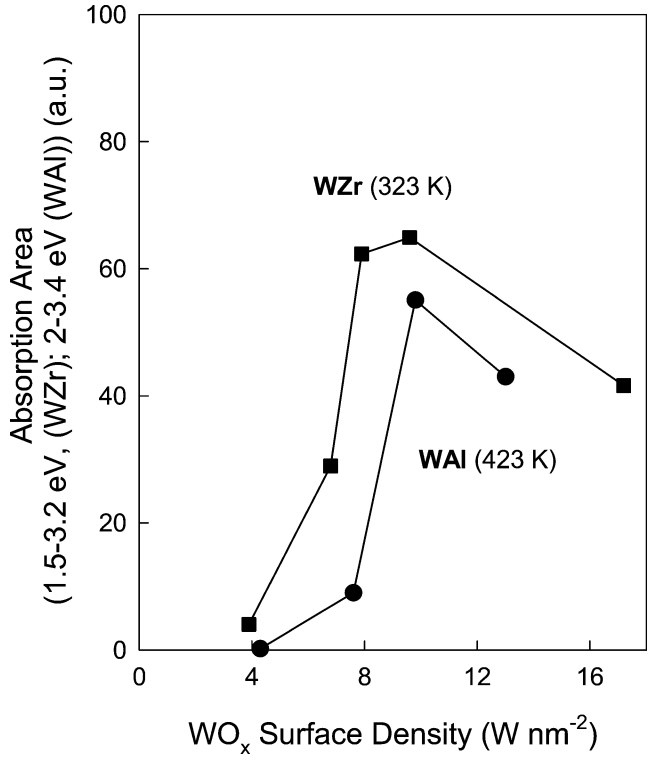

Fig. 13. Integrated UV–vis absorption area corresponding to the data presented in Fig. 12) of WAl (423 K) and WZr (323 K) as a function of WO_x surface density. Catalysts shown: WAl (●) and WZr (■). [Spectra are obtained after 1 h during steady-state reaction with 2-butanol (0.5 kPa 2-butanol), absorption areas were integrated from 1.5–3.2 eV (WZr, Fig. 12a) and 2–3.4 eV (WAl, Fig. 12b).]

groups with Brønsted acid character. The parallel evolution of catalytic dehydration rates (Fig. 3), Brønsted acid site density (Fig. 7a), and extent of reduction for WAl (Fig. 13) (these data are summarized in Table 3) at surface densities from 4.3 W to 9.8 W nm^{-2} indicate that $H^{\delta+}(WO_3)_n{}^{\delta-}$ centers act as Brønsted acid sites; their properties resemble those reported for similar structures on WZr [16].

WAl samples showed fewer reduced centers than WZr, even at their higher reaction temperatures. This is consistent with their lower catalytic reactivity, which reflects the presence of fewer $H^{\delta+}(WO_3)_n{}^{\delta-}$ Brønsted acid sites. The extent of reduction and the density of these $H^{\delta+}(WO_3)_n{}^{\delta-}$ species depend sensitively on the support, which influences the ability of WO_x domains to delocalize charge. These UV–vis spectra and titration data lead us to conclude that Brønsted acid centers form on WAl via reduction processes previously shown to occur on WZr and that these pathways and the consequent support effects observed are common among acid catalysts based on neutral WO_x domains.

3.4. Support effects on alcohol dehydration turnover rates

Here, we return to the kinetics and mechanism of 2-butanol dehydration and show that dehydration turnover rates, rate constants for required kinetically relevant steps, and the reactivity of Brønsted acid sites are not affected by the identity of the supports. Dehydration turnover rates can be obtained from the measured rates (per W atom) and the number of Brønsted acid sites measured by 2,6-di-*tert*-butylpyridine titration. The effects of support on the intrinsic reactivity of these acid sites can be determined form these estimates.

Reaction rates from Eq. (1) and extrapolated to zero conversion ($\alpha[H_2O]/[A] \ll 1$) give the expression:

$$k' = \frac{k_2[L]}{1 + k_2/k_3} = r_0. \tag{2}$$

Thus, measured k_{app} values equal turnover rates (ν) for zero-order conversion of 2-butanol to butenes.

$$\frac{r_0}{[L]} = k_{app} = \nu. \tag{3}$$

We note that k_{app} depends on the ability of sites to react in E2 elimination (k_2) (Step 2 (Scheme 1)) and water desorption (k_3) (Step 3 (Scheme 1)) reactions, both of which can depend on acid strength. In Fig. 14, 2-butanol dehydration rates (per W atom) on WZr, WAl, WSi, and WSn are shown as a function of Brønsted acid site density (per W atom). These rates include only contributions from Brønsted acid sites; small contributions from Lewis acid sites were rigorously subtracted, using procedures described earlier. The data in Fig. 14 and Table 4 lie along a unique single curve for WO_x domains on all supports; the concave upward char-

Table 3
Initial dehydration rate, Brønsted acid site density, and relative abundance of reduced centers as a function of WO_x surface density for WAl catalysts

WO_x surface density (W nm^{-2})	Acid site characterization parameter		
	Initial dehydration rate[a] (10^{-4} s^{-1})	Brønsted acid site density[b] (H^+/W atom)	Relative abundance of reduced centers[c] (a.u.)
13	0.9	0.006	42.6
9.8	7.6	0.028	55.0
7.6	4.5	0.021	9.1
4.3	2.2	0.011	0.2

[a] Per W atom, for 2-butanol dehydration at 373 K, extrapolated to zero conversion.
[b] Determined from titration with 2,6-di-*tert*-butylpyridine during 2-butanol dehydration reaction at 373 K.
[c] Relative (ratio of integrated peak area of the different samples to the total area of Fig. 12b) UV–visible absorption area from 2 to 3.4 eV during 2-butanol dehydration at 423 K.

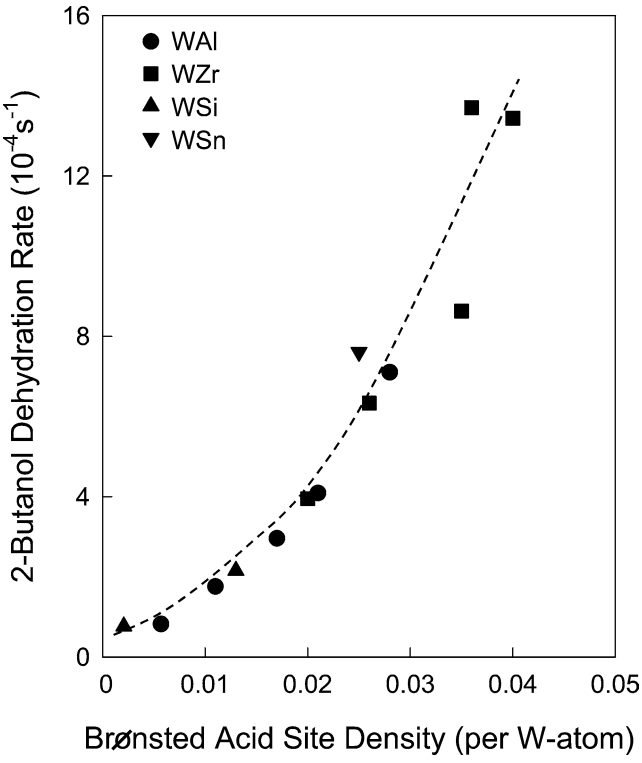

Fig. 14. Dehydration rates (per W atom) as a function of Brønsted acid site density. Initial dehydration rates were determined by 2-butanol dehydration reactions. Dehydration rates are dehydration rates extrapolated to zero conversion less residual rates (on Lewis acid sites). The error introduced by taking the residual rates without extrapolation to zero reactant conversion is assumed to be minimal, since these rates were obtained at very low conversions. Brønsted acid site densities were determined by titration with 2,6-di-*tert*-butylpyridine. Different catalysts are shown: WAl (●), WZr (■), WSi (▲), and WSn (▼).

acter of this curve indicates that turnover rates increase with increasing density of acid sites on all supports.

A rearrangement of Eq. (2) illustrates the possible effects of acid strength on measured turnover rates:

$$\upsilon = \frac{k_2}{1 + k_2/k_3} = \frac{1}{1/k_2 + 1/k_3}. \quad (4)$$

Higher values of either k_2 or k_3 would lead to higher dehydration turnover rates. We cannot unequivocally attribute the apparent increase in reactivity to changes in either rate constant, because their relative contributions are unknown. It is tempting to suggest that weaker acid sites, prevalent as samples must delocalize additional charge with increasing site density (per W atom), lead to faster rates for steps 2 and 3 in the mechanistic scheme. We cannot rule out, however, that the observed curvature merely reflects an overestimate of active Brønsted acid densities at low WO_x surface densities, because titrants may also interact with permanent but less reactive Brønsted acid sites. These sites may consist of protons required to balance the negative charge in minority W–O–M structures (M = support cation) near the periphery of isolated monotungstates or small polytungstate domains.

4. Conclusions

2-Butanol dehydration rates and the density of Brønsted and Lewis acid sites of several WAl and WSi samples and one WSn sample were determined. On WAl, 2-butanol dehydration rates (per W atom) increased with increasing WO_x surface density and reached maximum values at WO_x surface densities (9–10 W nm^{-2}) similar to those required for two-dimensional polytungstates, as also found previously on WZr. With increasing WO_x surface density, UV–vis edge energies decrease on WAl and WZr, suggesting an increase in WO_x domain size. Selective titration of Brønsted acid sites by sterically hindered 2,6-di-*tert*-butylpyridine during 2-butanol dehydration reaction showed that this reaction occurs predominately on Brønsted acid sites for WO_x domains supported on ZrO_2, Al_2O_3, SiO_2, and SnO_2. Preedge features appear in the UV–vis spectra of WAl samples dur-

Table 4
Brønsted acid site densities, corrected dehydration rates, and dehydration turnover rates on WZr, WAl, WSi, and WSn

Catalyst	Brønsted acid site density[a] (H^+/W atom)	Corrected dehydration rate[b] (10^{-4} s^{-1})	Dehydration turnover rate[c] (10^{-4} s^{-1})
W(3.9)Zr	0.020	3.95	198
W(6.8)Zr	0.040	13.44	336
W(9.6)Zr	0.036	13.70	381
W(14.8)Zr	0.035	8.63	246
W(17.2)Zr	0.026	6.33	244
W(4.3)Al	0.011	1.76	160
W(5.8)Al	0.017	2.96	174
W(7.6)Al	0.021	4.09	195
W(9.8)Al	0.028	7.10	254
W(13)Al	0.006	0.82	137
W(6.5)Si	0.013	2.16	166
W(23)Si	0.002	0.77	385
W(7.7)Sn	0.025	7.60	304

[a] Per W atom, for 2-butanol dehydration at 373 K.
[b] Corrected rates represent dehydration rates extrapolated to zero conversion diminished by the residual rates (Table 2) determined from titration with 2,6-di-*tert*-butylpyridine during reaction with 2-butanol at 373 K.
[c] [Molecules 2-butanol converted/per Brønsted acid site (determined from 2,6-di-*tert*-butylpyridine titration at 373 K)/s].

ing 2-butanol dehydration and their intensity increases with WO_x surface density in parallel with measured Brønsted acid site densities and dehydration rates (per W atom). These preedge features reflect the formation of reduced centers, consisting of acidic $H^{\delta+}(WO_3)_n{}^{\delta-}$ species, using 2-butanol as a stoichiometric reductant. These processes resemble those on WZr, indicating that temporary acid sites generally form from neutral WO_x precursors on all supports. The in situ formation of these active sites is underlined by the temperature dependence of Brønsted acid site density. Dehydration turnover rates (per Brønsted acid site) were unaffected by the identity of the support, but for a given WO_x surface density, the number of reduced centers and the density of Brønsted acid sites, but not their intrinsic reactivity, depend on the identity of the support. As a result of electronic isolation of WO_x domains on the more insulating and unreducible Al_2O_3 supports, both reduced centers and Brønsted acid sites are more abundant on ZrO_2-supported than on Al_2O_3-supported samples. In contrast to dehydration turnover rates, dehydration regioselectivity on Brønsted acid sites is strongly influenced by support, with more electropositive support cations leading to stronger interactions between α-hydrogens in reactants and lattice oxygens favoring sterically hindered transition states required for the formation of *cis*-2-butene.

Acknowledgments

J.M. gratefully acknowledges the receipt of a scholarship of the Ernest-Solvay Stiftung. Support by the Chemical Sciences, Geo Sciences, Bio Sciences Division, Office of Basic Energy Sciences, Office of Science US department of Energy under Grant DE-FG02-03ER15479 is gratefully acknowledged.

Appendix

The following formula was used to define Brønsted acid site selectivities (S_{BA}):

$$S_{BA} = \left(\frac{r_{cis}^{initial} - r_{cis}^{final}}{r_{trans}^{initial} - r_{trans}^{final}} \right),$$

where $r_{cis}^{initial}$ and $r_{trans}^{initial}$ are the initial *cis*-2-butene and *trans*-2-butene formation rates, and r_{cis}^{final} and r_{trans}^{final} are the final *cis*-2-butene and *trans*-2-butene formation rates measured after all Brønsted activity has been suppressed by 2,6-di-*tert*-butylpyridine.

References

[1] M. Hino, K. Arata, J. Chem. Soc., Chem. Commun. (1987) 1259.
[2] M. Scheithauer, R.K. Grasselli, H. Knözinger, Langmuir 14 (1998) 3019.
[3] M. Scheithauer, T.K. Cheung, R.E. Jentoft, R.K. Grasselli, B.C. Gates, H. Knözinger, J. Catal. 180 (1998) 1.
[4] G. Larsen, E. Lotero, R.D. Parra, Stud. Surf. Sci. Catal. 101 (1996) 543.
[5] G. Larsen, E. Lotero, S. Raghavan, R.D. Parra, C.A. Querini, Appl. Catal. A 139 (1996) 201.
[6] G. Larsen, S. Raghavan, M. Márquez, E. Lotero, Catal. Lett. 37 (1996) 57.
[7] J.G. Santiesteban, J.C. Vartuli, S. Han, R.D. Bastian, C.D. Chang, J. Catal. 168 (1997) 431.
[8] D.G. Barton, M. Shtein, R.D. Wilson, S.L. Soled, E. Iglesia, J. Phys. Chem. B 103 (1999) 630.
[9] D.G. Barton, S.L. Soled, G.D. Meitzner, G.A. Fuentes, E. Iglesia, J. Catal. 181 (1999) 52.
[10] D.S. Kim, M. Ostromecki, I.E. Wachs, J. Mol. Catal. A 106 (1996) 93.
[11] S.L. Soled, G.B. McVicker, L.L. Murrell, L.G. Sherman, N.C. Dispenziere, S.L. Hsu, D. Waldman, J. Catal. 111 (1988) 286.
[12] A. Gutiérrez-Alejandre, P. Castillo, P. Ramírez, G. Ramis, G. Busca, Appl. Catal. A. 216 (2001) 181.
[13] L.H. Gielgens, M.G.H. van Kampen, M.M. Broek, R. van Hardeveld, V. Ponec, J. Catal. 154 (1995) 201.
[14] V.M. Benitez, C.A. Querino, N.S. Fígoli, R.A. Comelli, Appl. Catal. A 178 (1999) 205.
[15] G.M. Maksimov, M.A. Fedotov, S.V. Bogdanov, G.S. Litvak, A.V. Golovin, V.A. Likholobov, J. Mol. Catal. A. 158 (2000) 435.
[16] C.D. Baertsch, K.T. Komala, Y.-H. Chua, E. Iglesia, J. Catal. 205 (2002) 44.
[17] C.D. Baertsch, S.L. Soled, E. Iglesia, J. Phys. Chem. B 105 (2001) 1320.
[18] R.D. Wilson, D.G. Barton, C.D. Baertsch, E. Iglesia, J. Catal. 194 (2000) 175.
[19] J.S. Beck, J.C. Vartuli, W.J. Roth, M.E. Leonowicz, C.T. Kresge, J. Am. Chem. Soc. 114 (1992) 10834.
[20] C.T. Kresge, M.E. Leonowicz, W.J. Roth, J.C. Vartuli, J.S. Beck, Nature 359 (1992) 710.
[21] X. Feng, G.E. Fryxell, L.Q. Wang, A.Y. Kim, J. Liu, K.M. Kemner, Science 276 (1997) 923.
[22] P. Kubelka, F.Z. Munk, Tech. Phys. 12 (1931) 593.
[23] H.C. Brown, R.B. Johanneson, J. Am. Chem. Soc. 75 (1953) 16.
[24] H.A. Benesi, B.H.C. Winquist, in: D.D. Eley, P.W. Selwood, P.B. Weisz (Eds.), in: Advances in Catalysis, vol. 27, Academic Press, New York, 1978, p. 97.
[25] P.A. Jacobs, C.F. Heylen, J. Catal. 34 (1974) 267.
[26] H. Knözinger, H. Buhl, K. Kochloefl, J. Catal. 24 (1972) 57.
[27] H. Noller, W. Kladning, Catal. Rev.-Sci. Eng. 13 (2) (1976) 179.
[28] H. Noller, K. Thomke, J. Mol. Catal. 6 (1979) 375.
[29] R.T. Sanderson, J. Chem. Ed. 65 (1988) 112.
[30] K. Chen, A.T. Bell, E. Iglesia, J. Catal. 209 (2002) 35.
[31] D. Masure, P. Chaquin, C. Louis, M. Che, M. Fournier, J. Catal. 119 (1989) 415.
[32] R.S. Weber, J. Catal. 151 (1995) 470.
[33] A. Khodakov, B. Olthof, A.T. Bell, E. Iglesia, J. Catal. 181 (1999) 205.
[34] J.A. Horsley, I.E. Wachs, J.M. Brown, G.H. Via, F.D. Hardcastle, J. Phys. Chem. 91 (1987) 4014.